Manuscript JOIV

by Sandino Sandino

Submission date: 02-Feb-2023 07:14PM (UTC+0700)
Submission ID: 2004732203
File name: Paper_Joiv_Sandino.pdf (4.17M)
Word count: 4246
Character count: 22555

JOIV : Int. J. Inform. Visualization, 6(4) - December 2022 755-762

INTERNATIONAL JOURNAL ON INFORMATICS VISUALIZATION

journal homepage : www.joiv.org/index.php/joiv

A Conversion of Signal to Image Method for Two-Dimension Convolutional Neural Networks Implementation in Power Quality Disturbances Identification

Sunneng Sandino Berutu [a], Yeong-Chin Chen [b], Heri Wijayanto [c,*], Haeni Budiati [a]

[a] Department of Informatika, Immanuel Christian University, Solo Rd, Yogyakarta, 55571, Indonesia
[b] Depatment of Computer Science and Information Engineering, Asia University, 500, Lioufeng Rd, Wufeng, Taichung, 41354, Taiwan
[c] Depatment of Informatika, University of Mataram, 62, Majapahit Rd, Mataram, Nusa Tenggara Barat, 83125, Indonesia
Corresponding author:*heri@unram.ac.id

***Abstract*—The power quality is identified and monitored to prevent the worst effects arise on the electrical devices. These effects can be device failure, performance degradation, and replacement of some device parts. The deep convolutional neural networks (DCNNs) method can extract the complexity of image features. This method is adopted for the power quality disruption identification of the model. However, the power quality signal data is a time series. Therefore, this paper proposes an approach for the conversion of a power quality disturbance signal to an image. This research is conducted in several stages for constructing the approach proposed. Firstly, the size of a matrix is determined based on the sampling frequency values and cycle number of the signal. Secondly, a zero-cross algorithm is adopted to specify the number of signal sample points inserted into rows of the matrix. The matrix is then converted into a grayscale image. Furthermore, the resulting images are fed to the two-dimension (2D) CNNs model for the PQDs feature learning process. When the classification model is fit, then the model is tested for power quality data prediction. Finally, the model performance is evaluated by employing the confusion matrix method. The model testing result exhibits that the parameter values such as accuracy, recall, precision, and f1-score achieve at 99.81%, 98.95%, 98.84, and 98.87 %, respectively. In addition, the proposed method's performance is superior to the previous methods.**

***Keywords*—Power quality disturbances; conversion; identification; convolutional neural network.**

Manuscript received 10 Jan. 2022; revised 22 Mar. 2022; accepted 14 Apr. 2022. Date of publication 31 Dec. 2022.

I. INTRODUCTION

Power quality is an important factor in the utilization of electrical devices. Power quality disturbances (PQDs) occur and cause negative effects such as failure, performance reduction, and maintenance costs for electrical equipment[1]. The PQDs categories are harmonic, sag, interruption, swell, notch, flicker, and transient[2]. The PQDs are caused by various loads [3], [4] such as arc generators, the converters of power, etc. Therefore, it is crucial to identify these disruptions as preventive steps and to minimize the worst effects.

Several researchers have adopted the deep learning method to identify the PQDs. Convolutional neural networks (CNNs) are mostly utilized methods for PQDs identification [1] and have received much attention due to their capability to learn the complexities of the image features [5]. In addition, this method also has low-cost computation at the model training phase [6]. The one-dimension(1D) [7]–[12] and 2D CNNs types [13]–[16] have been implemented for the detection and classification of the PQDs where the 1D CNNs learn time-series data while the 2D CNNs are image data. The image is obtained from the conversion of time-series signal data.

Several authors have introduced conversion methods in this field. In these methods, the concept of trajectory matrix was utilized in the conversion process [5]. The quadratic mean was adopted to capture the signal event as the image [17]. The spectrogram and scalogram approaches have been also applied [18], [19]. Furthermore, some previous studies [20]–[22] employed the space phasor diagram. However, these conversion methods entirely changed the authentic data value, so the image is unrepresented in the whole signal. The other methods created the rectangular matrix from the sample values of the signal [23]–[25]. The matrix was then converted to a grayscale image. However, these methods only transfer 80 to 90 percent of the number of samplings into the matrix. In

addition, the matrix size determination is also unexplained detailly in their papers. Therefore, we proposed a conversion method where the matrix size determination refers to the number of cycles. This approach also adopts the zero-cross algorithm to specify the position of the signal samplings in the matrix.

II. Materials and Methods

This section presents the disturbances data source, the proposed conversion method, the design of model architecture, and the model evaluation.

A. Power Signal Disturbance Data

The disturbance signal dataset is synthetic [17], [18], [20]–[26] [10-18] generated by applying the formula[27] in Table 1. The parameters in this equation are referred to the IEEE standard [28]. In this study, there are 12 disturbances categories such as flicker, swell, sag, harmonic, flicker harmonic, sag harmonic, swell harmonic, flicker sag, flicker swell, interruption, interruption harmonic, and normal. The parameters of the values of fundamental (f) and sampling frequencies (fs) are 60 Hz and 3200 Hz, respectively[8].

TABLE I
THE FORMULA OF SYNTHETIC DATA

Disruption Category	Formula	Parameter
C1-Normal	$y(t) = A[1 \pm \beta(u(t-t_a) - u(t-t_b))]sin(\alpha t)$	$\beta \le 0.1$, $T \le t_b - t_a \le 9T$, $\alpha = 2\pi f$
C2-Flicker	$y(t) = A[1 + \gamma sin(\alpha_f t)]sin(\alpha t)$	$8 \le f_f \le 25\ Hz$, $\alpha_f = 2\pi f_f$ $0.05 \le \gamma \le 0.1$
C3-Flickerharmonic	$y(t) = A[1 + \gamma sin(\alpha_f t)][\beta_1 sin(\alpha t) + \beta_3 sin(3\alpha t) + \beta_5 sin(5\alpha t)]$	$0.05 \le \gamma \le 0.1$, $8 \le f_f \le 25\ Hz$, $0.05 \le \beta_3, \beta_5, \beta_7 \le 0.15$, $\sum \beta_i^2 = 1$
C4-Flickersag	$y(t) = A[1 + \gamma sin(\alpha_f t)(1 - \beta(u(t-t_a) - u(t-t_b))]sin(\alpha t)$	$0.1 \le \beta \le 0.9$, $T \le t_b - t_a \le 9T$, $0.05 \le \gamma \le 0.1$, $8 \le f_f \le 25\ Hz$
C5-Flickerswell	$y(t) = A[1 + \gamma sin(\alpha_f t)(1 + \beta(u(t-t_a) - u(t-t_b))]sin(\alpha t)$	$0.1 \le \beta \le 0.8$, $T \le t_b - t_a \le 9T$, $0.05 \le \gamma \le 0.1$, $8 \le f_f \le 25\ Hz$
C6-Harmonic	$y(t) = A[\beta_1 sin(\alpha t) + \beta_3 sin(3\alpha t) + \beta_5 sin(5\alpha t) + \beta_7 sin(7\alpha t)]$	$0.05 \le \beta_3, \beta_5, \beta_7 \le 0.15, \sum \beta_i^2 = 1$
C7-Interruption	$y(t) = A[1 - \beta(u(t-t_a) - u(t-t_b))]sin(\alpha t)$	$0.9 \le \beta \le 1$, $T \le t_b - t_a \le 9T$
C8-Interruptionharmonic	$y(t) = A[1 - \beta(u(t-t_a) - u(t-t_b))][\beta_1 sin(\alpha t) + \beta_3 sin(3\alpha t) + \beta_5 sin(5\alpha t)]$	$0.9 \le \beta \le 1$, $T \le t_b - t_a \le 9T$ $0.05 \le \beta_3, \beta_5, \beta_7 \le 0.15$, $\sum \beta_i^2 = 1$
C9-Sag	$y(t) = A[1 - \beta(u(t-t_a) - u(t-t_b))]sin(\alpha t)$	$0.1 \le \beta \le 0.9$, $T \le t_b - t_a \le 9T$
C10-Sagharmonic	$y(t) = A[1 - \beta(u(t-t_a) - u(t-t_b))][\beta_1 sin(\alpha t) + \beta_3 sin(3\alpha t) + \beta_5 sin(5\alpha t)]$	$0.1 \le \beta \le 0.9$, $T \le t_b - t_a \le 9T$, $0.05 \le \beta_3, \beta_5, \beta_7 \le 0.15$, $\sum \beta_i^2 = 1$
C11-Swell	$y(t) = A[1 + \beta(u(t-t_a) - u(t-t_b))]sin(\alpha t)$	$0.1 \le \beta \le 0.8$, $T \le t_b - t_a \le 9T$
C12-Swellharmonic	$y(t) = A[1 + \beta(u(t-t_a) - u(t-t_b))][\beta_1 sin(\alpha t) + \beta_3 sin(3\alpha t) + \beta_5 sin(5\alpha t)]$	$0.1 \le \beta \le 0.8$, $T \le t_b - t_a \le 9T$ $0.05 \le \beta_3, \beta_5, \beta_7 \le 0.15$, $\sum \beta_i^2 = 1$

In addition, the other parameters value, such as the flicker distortion (γ), the intensity (β), the time start(ta), and the end of disturbance (tb) are randomly produced. We generated the disturbance signals in the simulation with 11,000 samples in each category, and the data is 132,000 signals.

B. The Signal to Image Conversion Method

The proposed method in this study refers to the approaches presented in Refs [24], [25]. These methods utilized the matrix for the conversion process. As shown in Fig 1, we proposed this method's first and second steps. The matrix dimension was specified according to the signal's number of cycles and sample points.

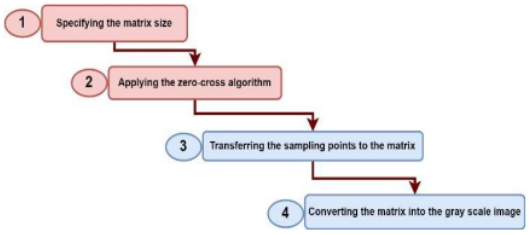

Fig. 1 A flowchart of the proposed conversion method

The details of the conversion method stages are explained as follows:

- Determining the dimension of matrix. The number of columns (*ncol*) and rows (*nr*) are obtained from the equation (1) and (2).

$$nr = nc * 2 \quad (1)$$

$$ncol = \frac{ns}{nr} \quad (2)$$

In this case, the number of cycles (*nc*) is at 11 with 586 sampling points (*ns*).

- Specifying the start and end points of a half cycle. The zero-cross algorithm [29] was adopted to determine the start and endpoints of a half-cycle of the signal illustrated in Fig 2.

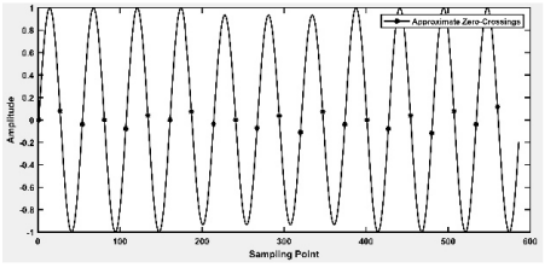

Fig. 2 Specifying a half-cycle the signal with the zero-cross algorithm

When the number of points in the half-cycle is less than the number of columns (*ncol)* value, the rest column will be filled with 0 value.

- Transfer the sampling values into the matrix. From step 2, we obtain each sampling point's row and column number, then the sampling point values are filled into the matrix. As a result, the positive sampling values appear in the odd rows in the matrix. The negative sampling values are in the even rows.
- Converting the matrix to image. The elements values of the matrix are converted into the grayscale color. The width and height of the image are obtained in the number of columns and rows of the matrix.

C. Deep CNN Architecture

The model architecture shown in Fig 3 contains four convolution layers with rectified linear unit (ReLU) activation, two max-pooling layers, and one dropout layer. Meanwhile, there are two dense layers for the classification, each utilizing the ReLU and the softmax activation functions.

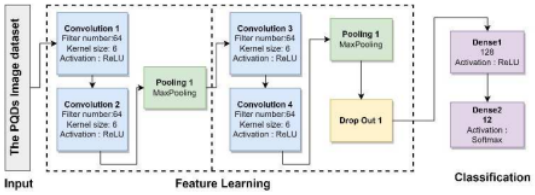

Fig. 3 The architecture of model deep CNN

D. Model Performance Evaluation

The confusion matrix is adopted to evaluate the performance of the model. From this matrix, the parameters of performance evaluation such as accuracy (A), precision (P), recall (R), and f1-score (f1) are obtained [30].

$$A = \frac{TP + TN}{TP + TN + FP + FN} \quad (1)$$

$$R = \frac{TP}{TP + FN} \quad (2)$$

$$P = \frac{TP}{TP + FP} \quad (3)$$

$$f1 = \frac{(2 * P * R)}{(P + R)} \quad (4)$$

Where TP is true positive, TN is true negative, FP is false negative, and FN is false negative[31].

III. Results and Discussion

This section presents the result of the proposed conversion method. The images resulting then are collected as a dataset. This dataset is fed to the 2D deep CNN model for features learning. Furthermore, the confusion matrix evaluates and analyses the model performance.

A. Conversion Result

The proposed method converted the disturbance signals produced from the formula in the Table 1 to the images. The image size resulting is 27 x 22 pixels with grayscale color. The images of each category are presented in Table 2. As mentioned in section two, the matrix contains the positive values in the odd rows. Meanwhile, the negative values are in the even rows. From the image, there are 22 grayscale shades where the odd lines are lighter than the even lines.

TABLE II
THE RESULT OF THE CONVERSION METHOD PROPOSED

Disturbance type	Grayscale Image	Disturbance type	Grayscale Image
C1-Normal		C7-Interruption	
C2-Flicker		C8-Interruptionharmonic	
C3-Flickerharmonic		C9-Sag	
C4-Flickersag		C10-Sagharmonic	
C5-Flickerswell		C11-Swell	
C6-Harmonic		C12-Swellharmonic	

B. Dataset Splitting

The images number of each disturbance category is 11,000. In this case, the total images obtained are 132,000 from the whole disturbance category. The model utilizes 120,000 images (80 % for the training and 20% for the validation) in the learning stage. Meanwhile, the rest is applied in the testing section. For the simulation, this study utilized three datasets presented in Table 3. The first dataset was obtained from the proposed conversion method. The second and third datasets have resulted from the conversion methods by authors in Refs [24], [25].

TABLE III
THE SIMULATION DATASETS

Conversion Method	Image Size (pixels)	Dataset Name
The proposed approach	27 x 22	D1
Author's approach in Ref[24]	24 x 24	D2
Author's approach in Ref[25]	30 x 20	D3

C. Model Learning

In this study, we employed three models with similar architecture as depicted in the Fig 3. The models are fed with three different datasets as described in the Table 3. The model names for the learning stage are presented in Table 4.

TABLE IV
THE MODEL NAMES

Model	Dataset
Model-D1	D1
Model-D2	D2
Model-D3	D3

TABLE V
THE MODEL LEARNING RESULT

Model	Accuracy (%)		Time Learning per epoch (s)
	Training	Validation	
Model-D1	98.80	99.31	26
Model-D2	98.61	98.82	23
Model-D3	98.00	98.11	26

For compile setting, the optimization algorithm utilized Adam with the learning rate at 0.001, whereas the categorical-cross-entropy was adopted for the loss function. In addition, the batch shape was set at 32. Meanwhile, we adjusted the epoch number to 100 for model fitting.

D. Model Testing

The model was evaluated to measure the PQDs classification performance. In the simulation, the models were tested with 12,000 images. The prediction results are presented in the confusion matrixes shown in Fig 4, 5, and 6.

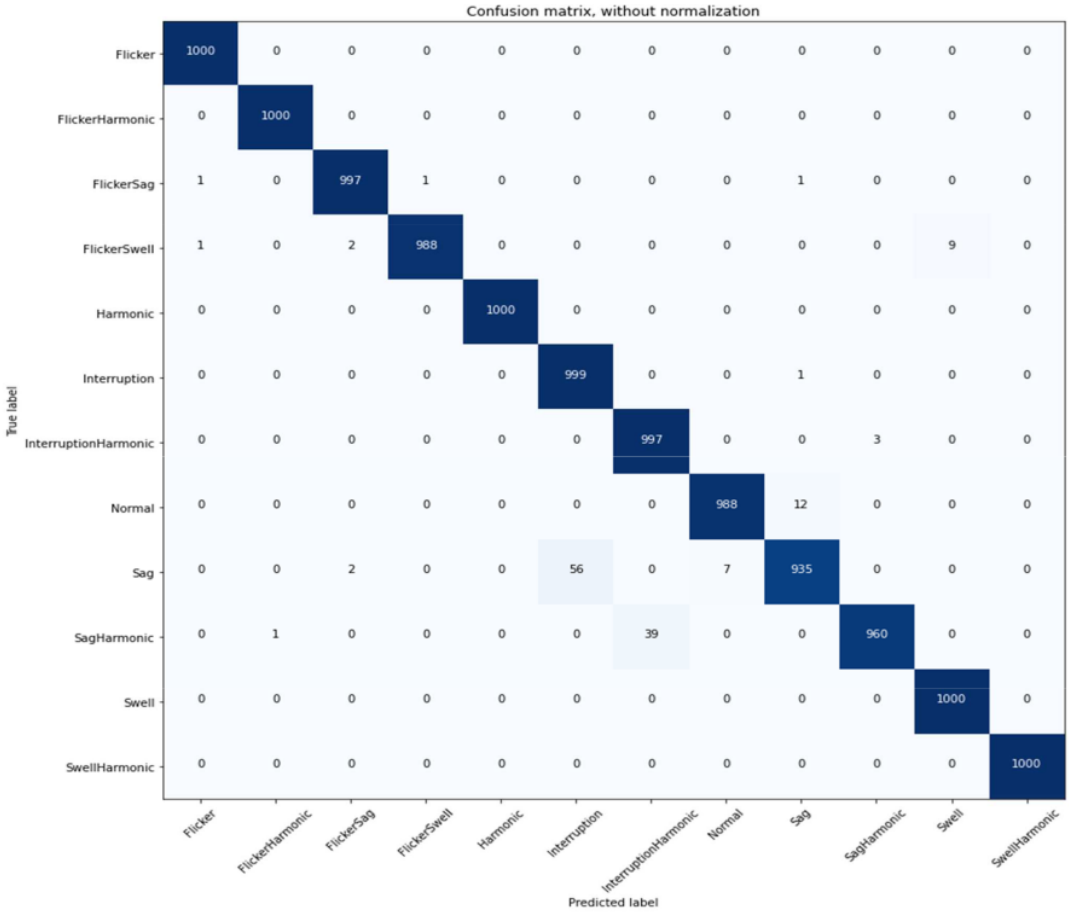

Fig. 4 The matrix confusion resulting from the Model-D1 learning

As displayed in Fig 4, the prediction result of the Model-D1 shows as five of the disturbance categories, such as C1-flicker, C2-flicker harmonic, C3-harmonic, C11-swell, and C12-swell harmonic, achieve the TP value at 1,000 images. On the other hand, the lowest TP value is the C9-sag type, with the FN value being 63 images. This type is detected in 56 images as the C7-interruption and in seven images as C1-normal.

Fig 5 shows the confusion matrix produced by the Model-D2 shows that five disturbance categories are C2-flicker, C6-harmonic, C1-normal, C11-swell, and C12-swellharmonic reach the TP value at 1,000 images. In contrast, the C5-flickerswell type obtains the lowest TP value with the FN value at 46 images. This type is recognized as the interruption at 41 images, two images as C2-flicker, and three as C4-flickersag.

The Fig 6 demonstrates the disturbance categories such as C3-flickerharmonic, C6-harmonic, and C12-swellharmonic with a TP value 1,000. Meanwhile, the C9-sag type obtains the lowest TP value, with the FN value at 56. This category is identified as C7-interruption with 43 images and 13 images as C1-normal.

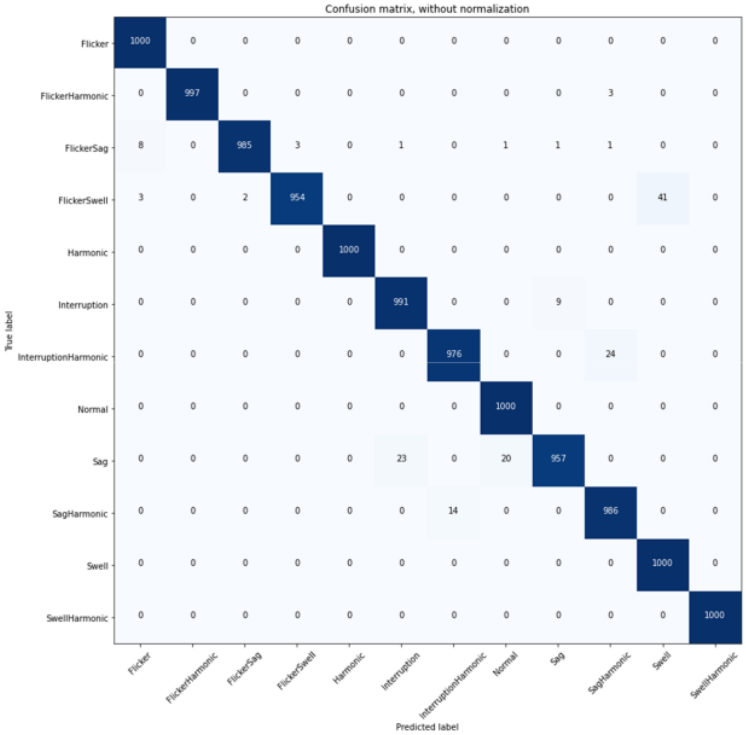

Fig. 5 The matrix confusion resulting from the Model-D2 learning

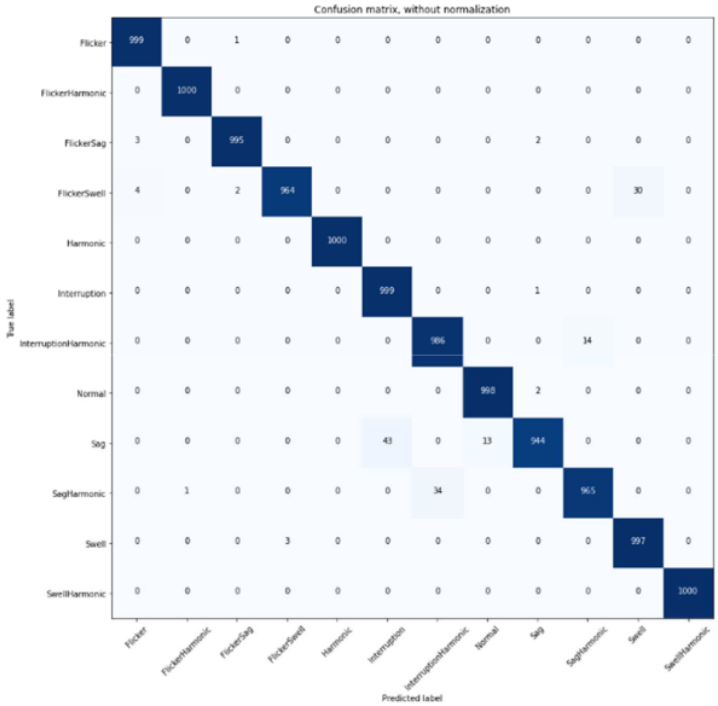

Fig. 6 The matrix confusion resulting from the Model-D3 learning

In general, these models result in the same TP for the category of C3-flickerharmonic, C6-harmonic, and C11-swell with value at 1,000. On the contrary, the C9-sag category obtains the lowest TP value with the highest FN values as the C7-interruption category. As shown in Table 1, the equation of the C9-sag and C7-interruption are similar, but the value of the intensity(β) variable is different. Therefore, when the intensity values of the C9-sag and C7-interruption are similar or closer, the features of C9-sag can be learned as the C7-interruption or vice versa.

The measuring accuracy, recall, precision, and the f1-score refer to the confusion matrixes in Fig 4, 5, and 6. The parameters measurement resulting from the model-D1, model-D2, and model-D3 are displayed in the bar graphs as shown in Figures 7,8, 9, and 10. In these graphs, the parameter values of each disturbance category are presented.

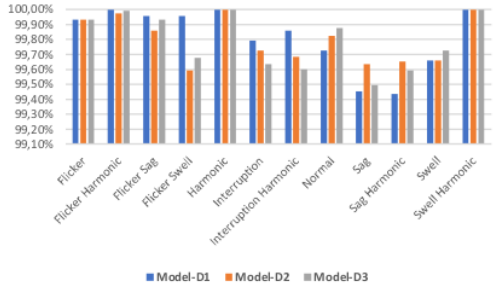

Fig. 7 The bar graph of the accuracy parameter of prediction in the model-D1, the model-D2, and the model-D3.

The Fig 7 demonstrates that the prediction accuracy of the model-D1 results in the highest value than the model-D2 and the model-D3 for the disturbance categories such as the C3-flickerharmonic, C4-flickersag, C5-flickerswell, C7-interruption, and C8-interruption harmonic. In addition, all models reach one hundred percent prediction value at the C11-swell and C6-harmonic categories.

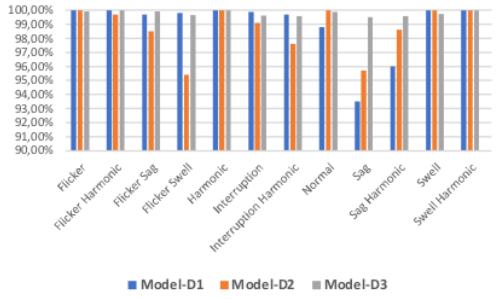

Fig. 8 The bar graph of the recall parameter of prediction in the model-D1, the model-D2, and the model-D3.

The bar graph in Fig 8 shows that the model-D1 has the highest value of the recall parameter in the disturbances type such as C2-flicker, C3-flickerharmonic, C5-flickerswell, C7-interruption, C8-interruptionharmonic, and C11-swell compared with the model-D2 and model-D3. In addition, the C6-harmonic and C12-swell harmonic disturbance types obtain a recall value of one hundred percent for all models.

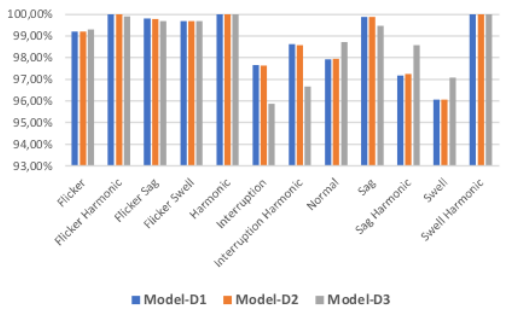

Fig. 9 The bar graph of the precision parameter of prediction in the model-D1, the model-D2, and the model-D3.

The bar graph Fig 9 illustrates that the parameter precision of model-D1 outperforms model-D2 and model-D3 for the disturbance categories such as the C4-flickersag and C8-interruption harmonic. In addition, model-D1 and model-D2 obtain a similar percentage in the C2-flicker, the C3-flicker harmonic, the C7-interruption, the C1-normal, the C9-sag, and the C11-swell. Furthermore, these models also achieve the precision value of one hundred percent at the C6-harmonic and the C12-swell harmonic categories.

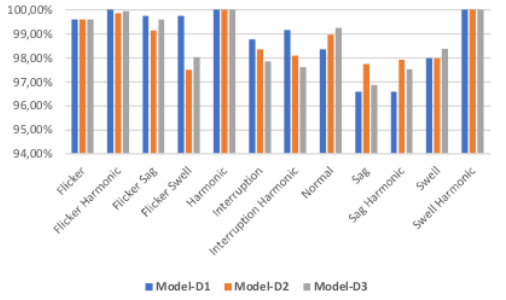

Fig. 10 The bar graph of the f1-score parameter of prediction in the model-D1, the model-D2, and the model-D3.

The bar graph of the f1-score in Fig 10 displays that model-D1 demonstrates superiority in the C4-flickersag, C5-flickerswell, C7-interruption, and C8-interruption harmonic over model-D2 and model-D3. In addition, the C6-harmonic and the C12-swell harmonic of all models obtain the f1-score one hundred percent. In general, the evaluation parameters of all models reach one hundred percent for the C6-harmonic and the C12-swell harmonic categories. The performance summary of the model-D1, the model-D2, and the model-D3 are presented in Table 6 and Fig 11.

TABLE VI
THE MODEL TESTING RESULT

Model	Accuracy (%)	Recall (%)	Precision (%)	F1-score (%)
Model-D1	99.81	98.95	98.84	98.87
Model-D2	99.79	98.71	98.83	98.76
Model-D3	99.78	98.72	98.74	98.72

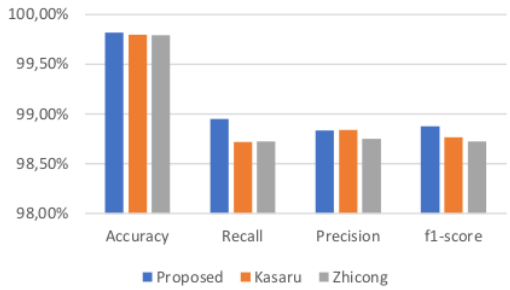

Fig. 11 The bar graph of the summary evaluation parameters of prediction in the model-D1, the model-D2, and the model-D3.

From Table 6, the performance of the proposed conversion approach (the model-D1) outperforms previous methods [17-18], where the evaluation parameters such as accuracy, recall, precision, and f1-score reach percentage values at 99.81, 98.95, 98.48, and 98.87, respectively. The parameters of the evaluation result are high (almost one hundred percent) because the data is synthetic and without noise in the signal. In addition, the categories of transient and notch disturbances are not included because the resulting image size is not similar to the others.

IV. Conclusion

The pre-processing data method for the conversion of the signal to the image is introduced in this study. In this proposed approach, the zero-cross algorithm is adopted for the sample points position determination of signal in the matrix. The conversion resulting is utilized as a dataset in the PQDs identification using the 2D CNNs algorithm. In the simulation, the evaluation showed that the percentage of the parameters such as accuracy, recall, precision, and f1-score reached 99.81, 98. 95, 98.84, and 98.87, respectively. In addition, the proposed conversion performance exceeds the existing approaches[24], [25]. For further research, this method will utilize the synthetic signal with noise. In addition, the ability of this approach can be evaluated using the actual signal data.

References

[1] M. Sahani, P. K. Dash, and D. Samal, "A real-time power quality events recognition using variational mode decomposition and online-sequential extreme learning machine," *Meas. J. Int. Meas. Confed.*, vol. 157, p. 107597, 2020, doi: 10.1016/j.measurement.2020.107597.

[2] P. Zhang, Q. Feng, R. Chen, D. Wang, and L. Ren, "Classification and Identification of Power Quality in Distribution Network," *2020 5th Int. Conf. Power Renew. Energy, ICPRE 2020*, no. 4, pp. 533–537, 2020, doi: 10.1109/ICPRE51194.2020.9233147.

[3] H. Sindi, M. Nour, M. Rawa, Ş. Öztürk, and K. Polat, "A novel hybrid deep learning approach including combination of 1D power signals and 2D signal images for power quality disturbance classification," *Expert Syst. Appl.*, vol. 174, no. November 2020, 2021, doi: 10.1016/j.eswa.2021.114785.

[4] P. Khetarpal and M. M. Tripathi, "A critical and comprehensive review on power quality disturbance detection and classification," *Sustain. Comput. Informatics Syst.*, vol. 28, p. 100417, 2020, doi: https://doi.org/10.1016/j.suscom.2020.100417.

[5] H. Liu, F. Hussain, Y. Shen, S. Arif, A. Nazir, and M. Abubakar, "Complex power quality disturbances classification via curvelet transform and deep learning," *Electr. Power Syst. Res.*, vol. 163, pp. 1–9, 2018, doi: https://doi.org/10.1016/j.epsr.2018.05.018.

[6] F. Nie, H. Wang, Q. Song, Y. Zhao, J. Shen, and M. Gong, "Image identification for two-phase flow patterns based on CNN algorithms," *Int. J. Multiph. Flow*, vol. 152, no. November 2021, p. 104067, 2022, doi: 10.1016/j.ijmultiphaseflow.2022.104067.

[7] S. Wang and H. Chen, "A novel deep learning method for the classification of power quality disturbances using deep convolutional neural network," *Appl. Energy*, vol. 235, no. November 2018, pp. 1126–1140, 2019, doi: 10.1016/j.apenergy.2018.09.160.

[8] Y. Shen, M. Abubakar, H. Liu, and F. Hussain, "Power quality disturbance monitoring and classification based on improved PCA and convolution neural network for wind-grid distribution systems," *Energies*, vol. 12, no. 7, 2019, doi: 10.3390/en12071280.

[9] A. Aggarwal, N. Das, M. Arora, and M. M. Tripathi, "A novel hybrid architecture for classification of power quality disturbances," *2019 6th Int. Conf. Control. Decis. Inf. Technol. CoDIT 2019*, pp. 1829–1834, 2019, doi: 10.1109/CoDIT.2019.8820557.

[10] N. Mohan, K. P. Soman, and R. Vinayakumar, "Deep power: Deep learning architectures for power quality disturbances classification," *Proc. 2017 IEEE Int. Conf. Technol. Adv. Power Energy Explor. Energy Solut. an Intell. Power Grid, TAP Energy 2017*, pp. 1–6, 2018, doi: 10.1109/TAPENERGY.2017.8397249.

[11] J. Wang, Z. Xu, and Y. Che, "Power Quality Disturbance Classification Based on Compressed Sensing and Deep Convolution Neural Networks," *IEEE Access*, vol. 7, pp. 78336–78346, 2019, doi: 10.1109/ACCESS.2019.2922367.

[12] S. S. Berutu and Y. C. Chen, "Power quality disturbances classification based on wavelet compression and deep convolutional neural network," *Proc. - 2020 Int. Symp. Comput. Consum. Control. IS3C 2020*, pp. 327–330, 2020, doi: 10.1109/IS3C50286.2020.00091.

[13] C. Chen, S. S. Berutu, Y. Chen, H. Yang, and C. Chen, "Regulated Two-Dimensional Deep Convolutional Neural Network-Based Power Quality Classifier for Microgrid," 2022.

[14] Y.-C. Chen, M. Syamsudin, and S. S. Berutu, "Pretrained Configuration of Power-Quality Grayscale-Image Dataset for Sensor Improvement in Smart-Grid Transmission," *Electronics*, vol. 11, no. 19, p. 3060, 2022, doi: 10.3390/electronics11193060.

[15] Y. Chen, S. S. Berutu, L. Hung, and M. Syamsudin, "A New Approach for Power Signal Disturbances Classification Using Deep Convolutional Neural Networks," vol. 24, no. 4, pp. 765–775, 2022, doi: 10.6633/IJNS.202207.

[16] Y. C. Chen, M. Syamsudin, and S. S. Berutu, "Regulated 2D Grayscale Image for Finding Power Quality Abnormalities in Actual Data," *J. Phys. Conf. Ser.*, vol. 2347, no. 1, 2022, doi: 10.1088/1742-6596/2347/1/012018.

[17] E. Balouji and O. Salor, "Classification of power quality events using deep learning on event images," *3rd Int. Conf. Pattern Anal. Image Anal. IPRIA 2017*, no. Ipria, pp. 216–221, 2017, doi: 10.1109/PRIA.2017.7983049.

[18] H. Xue, A. Chen, D. Zhang, and C. Zhang, "A Novel Deep Convolution Neural Network and Spectrogram Based Microgrid Power Quality Disturbances Classification Method," *Conf. Proc. - IEEE Appl. Power Electron. Conf. Expo. - APEC*, vol. 2020-March, pp. 2303–2307, 2020, doi: 10.1109/APEC39645.2020.9124252.

[19] S. K. G. Manikonda, S. Gangwani, S. P. K. Sreckala, J. Santhosh, and D. N. Gaonkar, "Power Quality Event Classification Using Convolutional Neural Networks on Images," *2019 IEEE 1st Int. Conf. Energy, Syst. Inf. Process. ICESIP 2019*, pp. 4–8, 2019, doi: 10.1109/ICESIP46348.2019.8938324.

[20] A. Bagheri, M. H. J. Bollen, and I. Y. H. Gu, "Improved characterization of multi-stage voltage dips based on the space phasor model," *Electr. Power Syst. Res.*, vol. 154, pp. 319–328, 2018, doi: 10.1016/j.epsr.2017.09.004.

[21] A. Bagheri, I. Y. H. Gu, M. H. J. Bollen, and E. Balouji, "A Robust Transform-Domain Deep Convolutional Network for Voltage Dip Classification," *IEEE Trans. Power Deliv.*, vol. 33, no. 6, pp. 2794–2802, 2018, doi: 10.1109/TPWRD.2018.2854677.

[22] F. Xiao, T. Lu, M. Wu, and Q. Ai, "Maximal overlap discrete wavelet transform and deep learning for robust denoising and detection of power quality disturbance," *IET Gener. Transm. Distrib.*, vol. 14, no. 1, pp. 140–147, 2020, doi: 10.1049/iet-gtd.2019.1121.

[23] S. Karasu and Z. Saraç, "Classification of power quality disturbances by 2D-Riesz Transform, multi-objective grey wolf optimizer and machine learning methods," *Digit. Signal Process. A Rev. J.*, vol. 101, p. 102711, 2020, doi: 10.1016/j.dsp.2020.102711.

[24] S. Karasu and Z. Saraç, "Investigation of power quality disturbances by using 2D discrete orthonormal S-transform, machine learning and multi-objective evolutionary algorithms," *Swarm Evol. Comput.*, vol.

44, no. January 2018, pp. 1060–1072, 2019, doi: 10.1016/j.swevo.2018.11.002.
[25] Z. Zheng, L. Qi, H. Wang, A. Pan, and J. Zhou, "Recognition method of voltage sag causes based on two-dimensional transform and deep learning hybrid model," *IET Power Electron.*, vol. 13, no. 1, pp. 168–177, 2020, doi: 10.1049/iet-pel.2019.0593.
[26] S. K. G. Manikonda, S. Gangwani, S. P. K. Sreckala, J. Santhosh, and D. N. Gaonkar, "Power Quality Event Classification Using Convolutional Neural Networks on Images," *2019 IEEE 1st Int. Conf. Energy, Syst. Inf. Process. ICESIP 2019*, pp. 0–4, 2019, doi: 10.1109/ICESIP46348.2019.8938324.
[27] R. Machlev, A. Chachkes, J. Belikov, Y. Beck, and Y. Levron, "Open source dataset generator for power quality disturbances with deep-learning reference classifiers," *Electr. Power Syst. Res.*, vol. 195, no. October 2020, p. 107152, 2021, doi: 10.1016/j.epsr.2021.107152.
[28] IEEE Std, *IEEE Recommended Practice for Monitoring Electric Power Quality*, vol. 2019. 1995. [Online]. Available: http://ieeexplore.ieee.org/xpl/freeabs_all.jsp?arnumber=5154067
[29] J. Brokešová and J. Málek, "Small-aperture seismic array data processing using a representation of seismograms at zero-crossing points," *Phys. Earth Planet. Inter.*, vol. 280, no. April, pp. 53–68, 2018, doi: 10.1016/j.pepi.2018.04.010.
[30] A. A. Hezam, S. A. Mostafa, Z. Baharum, A. Alanda, and M. Z. Salikon, "Combining Deep Learning Models for Enhancing the Detection of Botnet Attacks in Multiple Sensors Internet of Things Networks," *Int. J. Informatics Vis.*, vol. 5, no. 4, pp. 380–387, 2021, doi: 10.30630/JOIV.5.4.733.
[31] H. S. Park and S. J. Yoo, "Early Dropout Prediction in Online Learning of University using Machine Learning," *Int. J. Informatics Vis.*, vol. 5, no. 4, pp. 347–353, 2021, doi: 10.30630/JOIV.5.4.732.

Manuscript JOIV

ORIGINALITY REPORT

13%	8%	10%	2%
SIMILARITY INDEX	INTERNET SOURCES	PUBLICATIONS	STUDENT PAPERS

MATCH ALL SOURCES (ONLY SELECTED SOURCE PRINTED)

5%

★ www.mdpi.com

Internet Source

Exclude quotes	On	Exclude matches	Off
Exclude bibliography	On		